SUBMITTED TO: 4th International Conference on
Synchrotron Radiation Instrumentation
Manchester England, 07-15 to 07-19, 1991

BNL--46654

DE92 002074

DISCLAIMER

This report was prepared as an account of work sponsored by an agency of the United States Government. Neither the United States Government nor any agency thereof, nor any of their employees, makes any warranty, express or implied, or assumes any legal liability or responsibility for the accuracy, completeness, or usefulness of any information, apparatus, product, or process disclosed, or represents that its use would not infringe privately owned rights. Reference herein to any specific commercial product, process, or service by trade name, trademark, manufacturer, or otherwise does not necessarily constitute or imply its endorsement, recommendation, or favoring by the United States Government or any agency thereof. The views and opinions of authors expressed herein do not necessarily state or reflect those of the United States Government or any agency thereof.

Optical Design and Performance of the X25 Hybrid Wiggler Beam Line at the NSLS*

Lonny E. Berman, J.B. Hastings,
Tom Oversluizen, and Martin Woodle

National Synchrotron Light Source
Brookhaven National Laboratory
Upton, New York 11973, USA

RECEIVED BY OSTI
OCT 30 1991

Abstract

The X25 beam line at the National Synchrotron Light Source (NSLS) began full-power commissioning in 1990. It extracts radiation from a 27 pole hybrid wiggler, which produces up to 1.8 kW of total power with a peak horizontal density of 450 W/mrad and critical energy of 4.6 keV. The design and performance of the beam line optics are described, in particular the cooling of the first monochromator crystal.

*SRI-91 oral contribution S11

*Work performed under the auspices of the U.S. Department of Energy, under contract DE-AC02-76CH00016.

MASTER

DISTRIBUTION OF THIS DOCUMENT IS UNLIMITED

I. Introduction

The X25 beam line at the NSLS has recently been commissioned. The radiation source is a 27 pole hybrid wiggler[1] installed in a straight section of the 2.5 GeV storage ring. The wiggler's field is approximately the same as that of a dipole bending magnet, hence the spectrum is similar to that from the bending magnet but more intense. The beam line optics consist of a 1:1 double-focussing mirror followed by a non-dispersive double crystal monochromator;[2] a subsequent dispersive monochromator can also be accomodated. The beam line can function with both the mirror and monochromator in place, either element in place, or neither one in place, and is therefore capable of delivering focussed or unfocussed white or monochromatic x-rays to the experimental hutch. This flexibility has already been used to advantage in several "flagship" experiments, spanning high power crystal optics testing,[3,4] white beam Laue protein crystallography,[5] coherent beam interference imaging of crystal domains,[6] and high energy resolution studies of absorption edge fine structure.[7] The experimental hutch has x-ray shielding and ozone removal[8] facilities robust enough to handle the full power white beam, and contains a dedicated six-circle diffractometer[9] on a kinematic table[10] for general high-q resolution scattering experiments.

This paper cribes the design and performance of the X25 optics, with an emphasis on the cooling of the first monochromator crystal.

II. Wiggler Source and Spectrum

The X25 hybrid wiggler's characteristics are described in Ref. 1. In brief, it is a 27 pole, 1.1 T device which uses samarium-cobalt magnet blocks and vanadium-permendur pole pieces. The length of a single period is 12 cm, giving a k-value of 12.3 and a characteristic horizontal opening angle of $\frac{k}{\gamma}$ = 2.5 mrad for a 2.5 GeV storage ring energy. The critical energy at the center of the horizontal fan is 4.6 keV. At a typical x-ray fill starting current of 230 mA, the wiggler produces 1.8 kW of total power with a central density of 450 W/mrad.

Components positioned in the front end of the beam line consist of a water-cooled copper mask followed by a fast vacuum valve, a twin-blade x-ray beam position monitor, a set of glancing-incidence adjustable apertures, and a tungsten-alloy x-ray shutter. These are identical to those used in the other x-ray insertion device front ends at the NSLS and have been described previously.[11]

A 0.25 mm thick beryllium window separates the storage ring from the beam line. Left unprotected, the window would absorb nearly half of the incident power. A set of 7 pyrolytic graphite foils, of 0.17 mm total thickness, is positioned immediately upstream of the window, to prevent it from absorbing excessive power.[12] The combination of the graphite foils and beryllium window reduces the central power density to 200 W/mrad at 230 mA, with most of the removed power from the soft end of the spectrum (below the critical energy). The foils themselves dissipate the absorbed power radiatively.

III. Mirror

The first optical element in the X25 beam line, positioned 14 m from the source, is a cylindrical platinum-coated silicon mirror[13] which is bent to a toroid. It has a fixed sagittal radius of 4.2 cm and an adjustable meridional radius, nominally set to 4600 m for a 3 mrad incidence angle and 1:1 focussing. Motorized linear vacuum feedthroughs[14] actuate the kinematic mounts on which the mirror assembly sits, and are used to adjust the mirror's position and incidence angle. Bending of the mirror is accomplished via application of torque couples at either end using cantilevered copper weights; the bending torque can be adjusted with a pair of high-resolution linear feedthroughs which apply spring pressure upward against the weights.[15] A water-cooled copper mask protects the upstream end of the mirror from errant x-rays.

At the mirror location, the peak horizontal power density can reach 14 W/mm, and the peak normal-incidence areal density can reach 4 W/mm^2. Since the mirror is positioned at a 3 mrad glancing angle to the incident beam, the heat load does not cause significant thermal distortions of the surface, even were the incident power totally absorbed. Hence the mirror is uncooled, and any residual power not reflected by the mirror is radiated from its polished surface. The 70 cm long mirror subtends approximately 1.5 mrad horizontally and 0.15 mrad vertically, in total about one-third of the available incident x-ray solid angle. It has a measured rms surface roughness of 10 Å,[16] and its x-ray reflectivity has been measured to be in excess of 80% at 8 keV, of

65% at 16 keV, and of 50% at 24 keV; the nominal cut-off energy is 28 keV. The mirror can provide up to 75 W of total white beam power in the experimental hutch (following transmission through two additional 0.25 mm thick beryllium windows) in a spot of FWHM dimension 0.80 mm horizontal by 0.45 mm vertical, giving a power density of over 200 W/mm^2! This is the highest x-ray power density readily available to a synchrotron radiation user.

IV. Monochromator

The monochromator, positioned 18 m from the source, consists of two non-dispersive silicon crystals affixed to a common rotary vacuum feedthrough which is actuated externally by a motorized tangent arm with a single-step resolution of 0.26 arcsec. The rotation is tracked with a precision encoder.[17] The feedthrough incorporates two teflon seals surrounding a transition space that can be pumped differentially. It has been found nevertheless that with use of a single viton o-ring which replaces the inside teflon seal, the vacuum integrity of the beam line (down to 10^{-8} Torr) can be maintained even as the feedthrough is scanned through its entire range, eliminating the need for differential pumping.[18] We have observed that the parallelism of the two crystals can be maintained to well within their narrowest fundamental Darwin reflection widths as the feedthrough traverses its range, due to the robust construction of the rotary spindle.

A unique feature of the monochromator is the mounting of the second crystal. It is clamped to a plate which is kinematically actuated using three vacuum-compatible piezoelectric inchworm

motors.[19] Together, they allow adjustment of the crystal's θ and χ orientations as well the gap between the surfaces of the two crystals. Each motor has a 6.5 mm travel range with a single-step resolution of 5 nm, resulting in a 15° range for θ and χ with a resolution of 0.02 arcsec. A schematic of the crystal assembly is included in Fig. 1. In normal operation, the rotation axis of the monochromator is coincident with the center of the first crystal's surface, where the white beam is incident. Hence the beam strikes the first crystal at the same position regardless of Bragg angle, but the diffracted beam walks along the long second crystal as the angle is scanned. This would cause the height of the doubly-diffracted beam to vary according to $2g\cos\theta_B$, where g is the gap between crystal surfaces and θ_B is the Bragg angle, but in practice this can be nulled by changing the gap as θ_B is scanned, so producing a fixed exit beam.

An x-ray shutter positioned downstream of the monochromator permits personnel access to the experimental hutch while maintaining incidence of the white beam on the first crystal, keeping it warm.

V. Crystal Cooling

At the monochromator location, the peak horizontal power density can reach 11 W/mm when the mirror is not used, and the peak normal-incidence areal density can reach 2.4 W/mm^2, increasing to about 4 W/mm^2 when the mirror is used. Since crystal Bragg angles are several degrees, the heat-loading problem on the first monochromator crystal is severe.

The thermal distortion problem which arises when the first crystal of a double crystal monochromator is subjected to a high power density x-ray beam, and various solutions, are discussed in detail in Ref. 20. In brief, tilt and dilational strains are introduced along the first crystal's diffracting surface (depicted graphically in Fig. 1), dispersing the diffracted x-rays in direction and wavelength so that they can no longer simultaneously satisfy the Bragg condition with the "cold" second crystal for any angular setting, entailing a loss of double-crystal-diffracted flux. In extreme cases, the monochromator's throughput saturates at a finite incident power level which corresponds to a fraction of the maximum stored current.[21] A simple solution, which preserves the total flux diffracted from the first crystal, is to remove the second crystal. Unfortunately, the deleterious effect of spoiling of the high brightness of the incident beam (the raison d'être of dedicated synchrotron radiation sources) remains, not to mention a degraded diffracted bandwidth compared with perfect optics. Whether or not a second crystal is used, it is imperative to pursue a first crystal cooling solution which minimizes the thermal distortion.

The crystal cooling concept which we have adopted is centered on the use of a free crystal lamella with the following characteristics: (1) the lamella is thin, to minimize the integrated thermal distortion along the diffracting surface,[22,23] (2) it is mounted in a strain-free manner, and (3) it can be simply upgraded to have provision for compensation of the residual thermal strain field.[24,25] The chosen cooling geometry involves removing the heat through the bottom of a silicon wafer ($\lesssim$1 mm

thick) which is set afloat a thin 75:25 gallium:indium liquid eutectic layer spread over a water-cooled copper block.[26] The eutectic layer serves both as a good thermal contact to the cooled base and a strain-free mount. It is vacuum-compatible, and since the water coolant does not make direct contact with the silicon, pressure-induced deformations[27] are non-existent; the wafer is held in place solely through the surface tension of the eutectic.

The setup shown in Fig. 1 was used to test the diffraction efficiency of the first monochromator crystal. The second crystal serves as a perfect analyzer, and by scanning its angle θ_2 while the first crystal angle θ_1 is held fixed, rocking curves can be recorded for the fundamental reflection using the ionization chamber D_1. If one places in front of a second chamber D_2 a suitable filter, which suppresses the fundamental reflection but transmits the first allowed harmonic at twice or thrice the photon energy of the fundamental, then rocking curves for the intrinsically narrower harmonic can be recorded simultaneously. Since the theoretical rocking curve widths are less than 2 arcsec for Si(333) and (440) harmonic reflections over the 3°-45° range of the monochromator, they provide a sensitive measure of thermal strain. The spatial distributions of strains (Bragg angle contours) can be mapped by scanning a narrow slit across the beam for given settings of θ_1 and θ_2;[28] again the resolution of the spatial mapping is improved by using the harmonic, since its narrower rocking curve width results in better contour resolution.[24]

The effect of crystal thickness on the diffraction efficiency was tested first. Rocking curve results for the (333) harmonic

reflection from a Si(111) crystal at 18.5 keV are shown in Fig. 2 for crystals of 1 and 2.5 mm thicknesses. These data were collected in the experimental hutch at 26 m from the source using the unfocussed beam, with a horizontal power density of 5 W/mm and a peak normal-incidence areal density of 0.8 W/mm^2 (180 mA current). Shown for comparison is a (333) rocking curve (similar for both thicknesses) for which the aluminum filter that normally sits in front of the harmonic detector was placed instead in the white beam, effectively eliminating the heat load. The latter reveals the rocking curve distortion arising from mounting strain and/or lack of crystal perfection, and, assuming a perfect unstrained analyzer, shows that the eutectic's surface tension broadens the observed rocking curve width from the intrinsic value of 0.8 arcsec to just 2 arcsec. For the thermally-distorted power-loaded crystals, increased thickness results in further reduction of peak intensity and increased rocking curve width, from 4 arcsec for the 1 mm thickness to 8 arcsec for the 2.5 mm thickness. This occurs because the incident synchrotron beam has a lateral (Gaussian) power profile, which gives rise to both a surface slope error variation and a Bragg angle variation due to the changing d-spacing, with magnitudes integrating with crystal thickness from the bottom.[22,23] Assuming one-dimensional heat flow, the surface slope error ("thermal bump") increases as the square of the thickness, and the d-spacing gradient increases linearly with the thickness; a different surface slope error, resulting from the bowing caused by the cooling gradient through the wafer, is independent of the thickness.[21-23] In conclusion, the crystal should be thin enough so that only the bowing

distortion remains significant. For the power densities encountered at the X25 beam line, the required thickness is $\lesssim 1$ mm for silicon at room temperature.

For use in the beam line (at 18 m from the source), 0.85 mm thick Si(111) and (220) first crystals were fabricated. Figure 3 shows rocking curves measured for the Si(220) fundamental reflection at 8 keV and the (440) harmonic at 16 keV, using the unfocussed beam. The horizontal power density was 8 W/mm and the peak normal-incidence areal density was 1.8 W/mm^2 (175 mA current). A heat-filtered (440) rocking curve is also shown. Comparison of this with theory shows that the mounting strain contribution to the rocking curve width was only 1.7 arcsec. For the power-loaded harmonic curve, there is an additional thermal strain contribution of 7.6 arcsec, assuming quadrature combination of the strain components. These reasonably account for the 50% additional width (compared with theory) of the observed fundamental curve. The vertical scales for these curves were chosen to conserve their areas, and suggest that the thermal distortion results in a loss of one-third of the ideal flux for the fundamental. The power-loaded fundamental and harmonic rocking curves both show a slight low-angle tail, indicating a residual d-spacing gradient contribution.[24]

More insight into the nature of the thermal strain can be gained by mapping the spatial distributions of diffracted intensity for different relative angle settings of the two crystals, using a 0.1 mm high scanning slit upstream of the ion chambers (Fig. 1). Figure 4 shows a series of such scans for the power-loading situation of Fig. 3. The solid and dashed curves in

the figure represent the distributions of Si(440) harmonic intensity; adjacent contours are separated by $\Delta\theta_2$ = 1 arcsec. Three Si(220) fundamental contours, separated by $\Delta\theta_2$ = 5 arcsec, are also shown. In the absence of any thermal and mechanical strains, all of the contours in the figure would be aligned (save for slight shifts due to beam steering), with widths determined by the Gaussian opening angle of the photon beam. The fact that the contours advance in position as the relative angle increases shows that the crystal surface is curved upwardly convex; the curvature radius is simply the rate of contour advance (in mm/arcsec) divided by $\sin\theta_B$.[24,27] Near the center of the beam (i.e., the central contours), the rate of advance is 0.6 mm/arcsec at the location of the slit, 27 m from the source, corresponding to a rate of 0.4 mm/arcsec at the monochromator, 18 m from the source. This gives a curvature radius of 200 m, which is more than twice the free wafer bowing radius expected from one-dimensional thermal diffusion theory for an input power density of 0.7 mm^2 along the top surface.[23] The disparity may derive from the fact that the simple theory applies to spherical bending (not cylindrical as is the case here), or that the mounting stiffens the crystal against bowing, or a combination of both.

Rocking curves identical to those of Fig. 3 were measured using the focussed beam, with a horizontal power density of 7 W/mm and a peak normal-incidence areal density of 2.7 W/mm^2 (150 mA current). This represents a similar horizontal density to the unfocussed case, but increased areal density. The increase in areal density arising from a shrinkage of the vertical dimension of the beam, for a given incident power, does not broaden the

observed rocking curve since, even though the thermal bowing radius (which is inversely proportional to the power density) decreases, there results a concomitant decrease in the length of the beam footprint (i.e., length of strain field sampled). From these data it can be concluded that, for fundamental x-ray reflections, the thin silicon crystal's diffraction performance is good for both the unfocussed and focussed incident power densities at X25.

The Bragg angle contours in Fig. 4 indicate that the first crystal of the monochromator has a curvature which is primarily convex cylindrical. In the next upgrade of the instrument, the crystal wafer will have a triangular shape, clamped at the base and pushed at the apex with a mechanical actuator, thus imparting a compensating concave cylindrical bend. This should recover not only the ideal fundamental intensity, but an ideal harmonic rocking curve as well; the latter is important for cases where harmonic rejection must be accomplished through a slight angular misaligment of the two crystals. Thermal contact between the bottom surface of the crystal wafer and the liquid eutectic can still be maintained even after "unbending" the wafer, since doing so displaces it away from the cooled copper block by just a few tenths of a micron.

VI. Summary

The optical design and performance of the X25 hybrid wiggler beam line at the NSLS have been described. Considerable flexibility has been built into the beam line to accomodate a wide

range of x-ray diffraction, imaging, scattering, and spectroscopy experiments with disparate requirements.

We have also demonstrated, for a typical incident x-ray power density level of present insertion device beam lines (~10 W/mm horizontal density, few W/mm^2 areal density, $\frac{1}{3}$ kW total power), that simple conduction cooling of a silicon crystal results in good x-ray diffraction efficiency if the crystal is thin and mounted in a strain-free manner. From the rocking curve dependence on crystal thickness shown in Fig. 2, plus the fact that the thermal curvature radius derived from the Bragg angle contour spacing in Fig. 4 is better (i.e., larger) than expected from simple thermal diffusion theory, it is clear that ideal diffraction behavior at room temperature is limited by the thermal-elastic response of the crystal to the power load, not by the heat transfer properties of the cooling system. It remains to be demonstrated, for the factor of 10-100 higher power densities which will be available at third-generation insertion device beam lines, whether the superior heat transfer properties of direct cooling schemes[3,21,27] will have impact on the diffraction performance of power-loaded silicon crystals, and also whether it will be necessary to lower silicon's thermal-elastic response sensitivity by, say, operating at cryogenic temperatures.[4]

Acknowledgements

Many individuals in the NSLS contributed tirelessly toward the design, construction, and commissioning of the X25 beam line. The commissioning of the wiggler itself necessarily preceded the

beam line commissioning, and was skillfully executed by the NSLS machine physics staff. This work was supported by the U.S. Department of Energy under Contract No. DE-AC02-76CH00016.

References

1. G. Decker, J. Galayda, L. Solomon, and M. Kitamura, Rev. Sci. Instrum. 60, 1845 (1989).

2. J. Hastings, B.M. Kincaid, and P. Eisenberger, Nucl. Instrum. Methods Phys. Res. 152, 167 (1978).

3. L.E. Berman and M. Hart, these Proceedings, contribution C5 (1992) and references therein.

4. G. Marot, A.K. Freund, M. Rossat, H. Kawata, S. Joksch, E. Ziegler, L.E. Berman, D. Chapman, J.B. Hastings, and M. Iarocci, these Proceedings, contribution C20 (1992).

5. P.T. Singer, R. Carty, L.E. Berman, and R.M. Sweet, to be published (1991).

6. M. Sutton, S.G.J. Mochrie, T. Greytak, S.E. Nagler, L.E. Berman, G.A. Held, and G.B. Stephenson, Nature 352, 608 (1991).

7. K. Hämäläinen, D.P. Siddons, J.B. Hastings, and L.E. Berman, to be published (1991).

8. N. Gmür, L.E. Berman, M. Iarocci, and C. Weilandics, National Synchrotron Light Source Technical Note 435 (1991).

9. Huber Diffraktionstechnik GmbH model 5020, Rimsting, Germany.

10. M. Iarocci, to be published (1992).

11. W. Thomlinson, D. Chapman, N. Gmür, and N. Lazarz, Nucl. Instrum. Methods Phys. Res., Sect. A 266, 226 (1988) and references therein.

12. E. Hoyer, Lawrence Berkeley Laboratory Engineering Note M6570A (1986).

13. The mirror was fabricated by Contraves USA, Boston Division (formerly Diamond Electro-Optics), Marlborough, Massachusetts.

14. T. Oversluizen, Vacuum 38, 27 (1988).

15. R. Hawrylak and S. Ulc, unpublished.

16. This was determined with a Wyko interferometer. We gratefully acknowledge Dr. Peter Takacz and his Optics Metrology Laboratory staff at Brookhaven for performing this measurement.

17. Heidenhain GmbH model ERO 725, Traunreut, Germany.

18. T. Oversluizen and P. Stefan, to be published (1992).

19. Burleigh Instruments model IW-700, Fishers, New York, USA.

20. L.E. Berman and M. Hart, Synchrotron Radiation News 4, no. 1, 22 (1991).

21. R.K. Smither, G.A. Forster, D.H. Bilderback, M. Bedzyk, K. Finkelstein, C. Henderson, J. White, L.E. Berman, P. Stefan, and T. Oversluizen, Rev. Sci. Instrum. 60, 1486 (1989).

22. S. Joksch, D. Degenhardt, R. Frahm, G. Meyer, and W. Jark, Nucl. Instrum. Methods Phys. Res., Sect. A 291, 325 (1990).

23. M. Hart, Nucl. Instrum. Methods Phys. Res., Sect. A 297, 306 (1990).

24. L.E. Berman and M. Hart, Nucl. Instrum. Methods Phys. Res., Sect. A 300, 415 (1991).

25. L.E. Berman and M. Hart, Nucl. Instrum. Methods Phys. Res., Sect. A 302, 558 (1991).

26. D.H. Bilderback, D.M. Mills, B.W. Batterman, and C. Henderson, Nucl. Instrum. Methods Phys. Res., Sect. A 246, 428 (1986).

27. T. Oversluizen, T. Matsushita, T. Ishikawa, P.M. Stefan, S. Sharma, and A. Mikuni, Rev. Sci. Instrum. 60, 1493 (1989).

28. L.E. Berman, unpublished.

Figure Captions

1. Experimental setup for diagnosing the thermal strains in the first monochromator crystal. The three inchworm motors used to orient the second crystal are also shown (the third motor is hidden behind the left one). The second crystal can be adjusted in Θ using the right motor alone, and in χ using the third (hidden) motor alone. Changing of the gap g is effected by scanning all three motors together.

2. Si(333) harmonic rocking curves measured from crystals with thicknesses of 1 mm and 2.5 mm, compared with a heat-filtered curve.

3. The upper panel shows a measured power-loaded Si(220) rocking curve at 8 keV using the unfocussed beam, compared with theory. The lower panel shows measured Si(440) rocking curves at 16 keV for the power-loaded and heat-filtered cases, compared with theory. The "gaps" in these rocking curves are artifacts introduced by the inchworm motor's clamping cycles.

4. Spatial distributions of diffracted intensity for the Si(220) fundamental and (440) harmonic reflections corresponding to the power-loaded case of Fig. 3. The harmonic contours, labelled 1-11 and alternately represented as solid and dashed curves, are separated in angle by $\Delta\Theta_2 = 1$ arcsec, with 1 the lowest and 11 the highest. Only the fundamental contours (chain-dashed) corresponding to harmonic contours 1, 6, and 11 are shown.

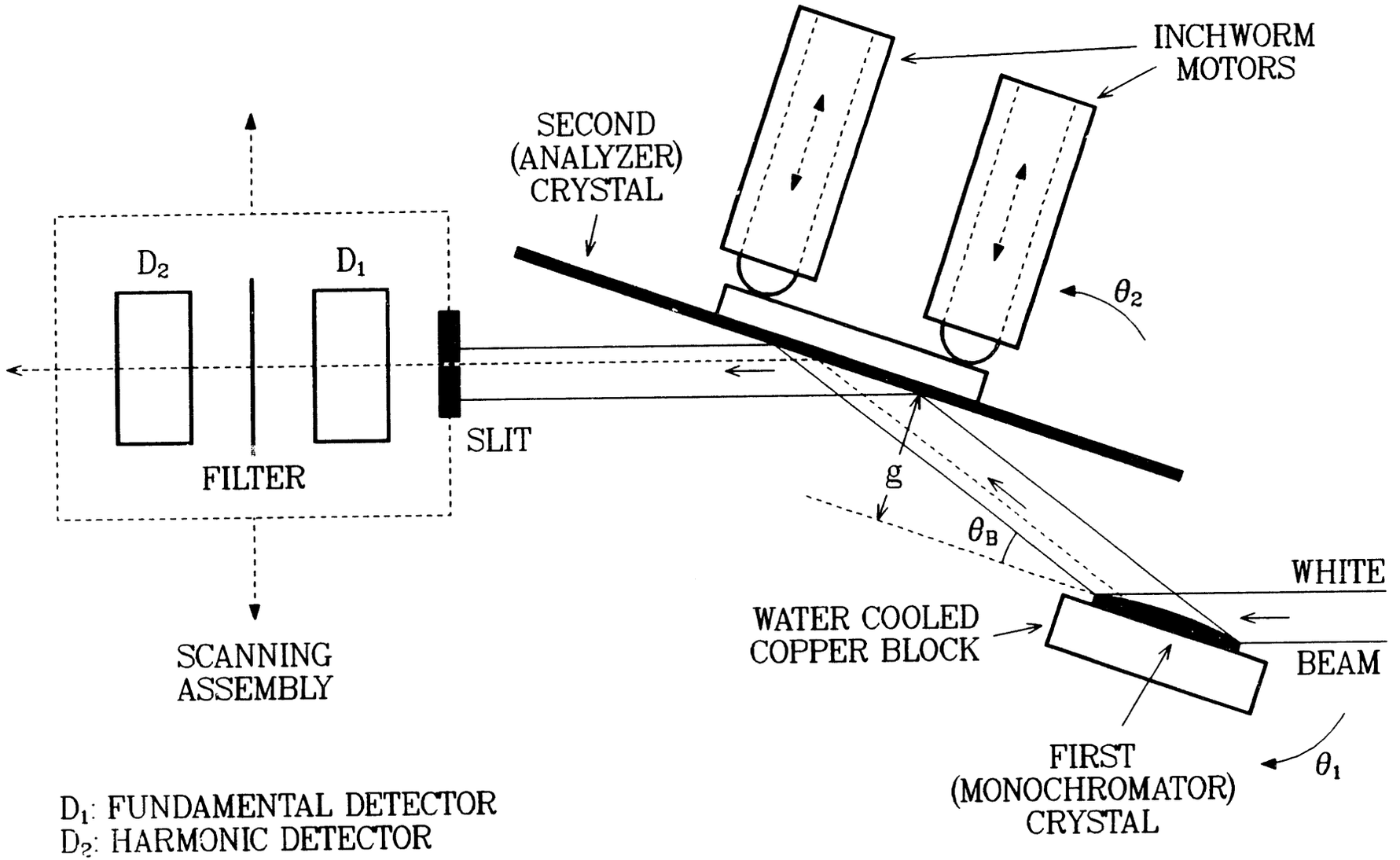

Berman et al., SRI-91 contribution S11, Figure 1

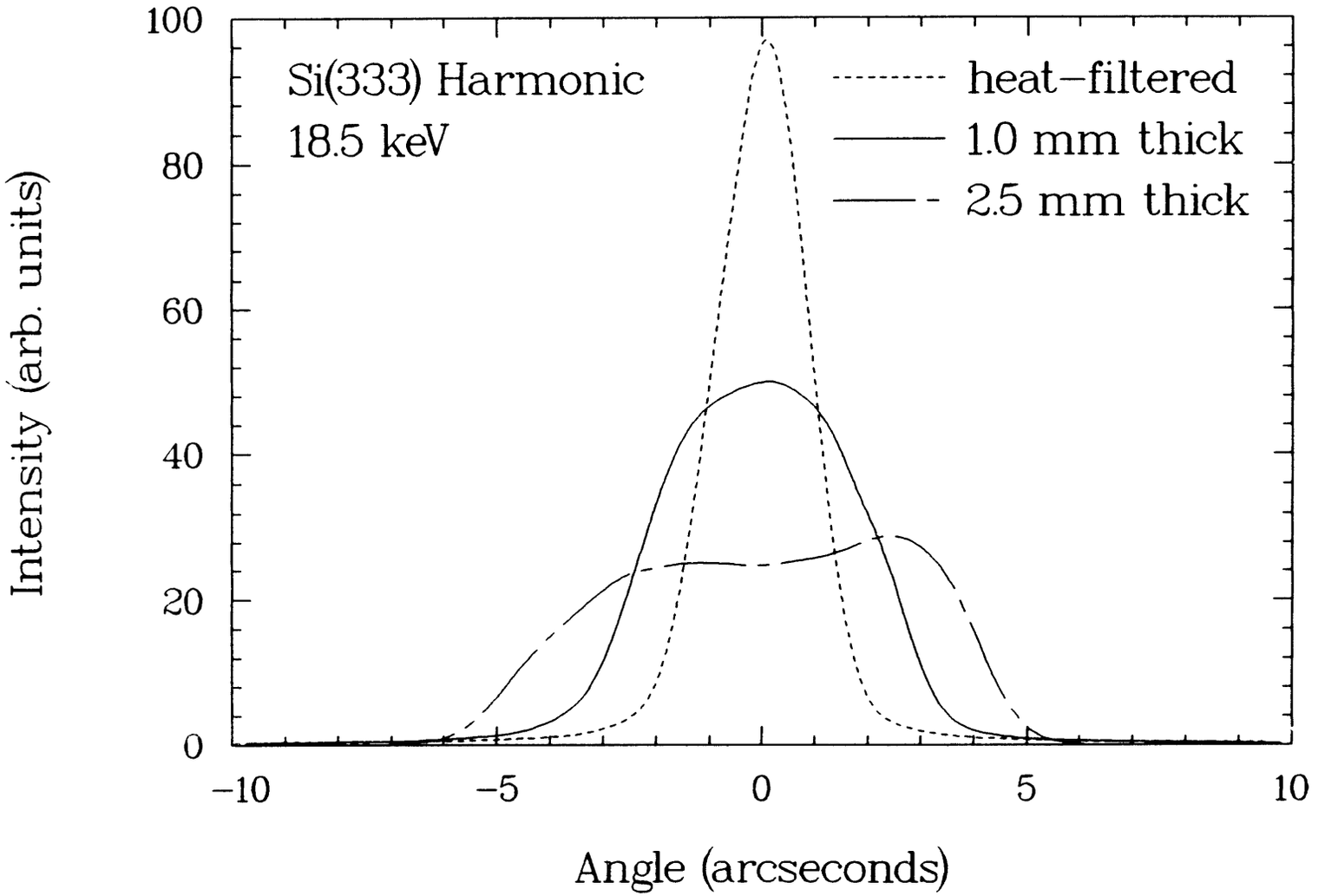

Berman et al., SRI–91 contribution S11, Figure 2

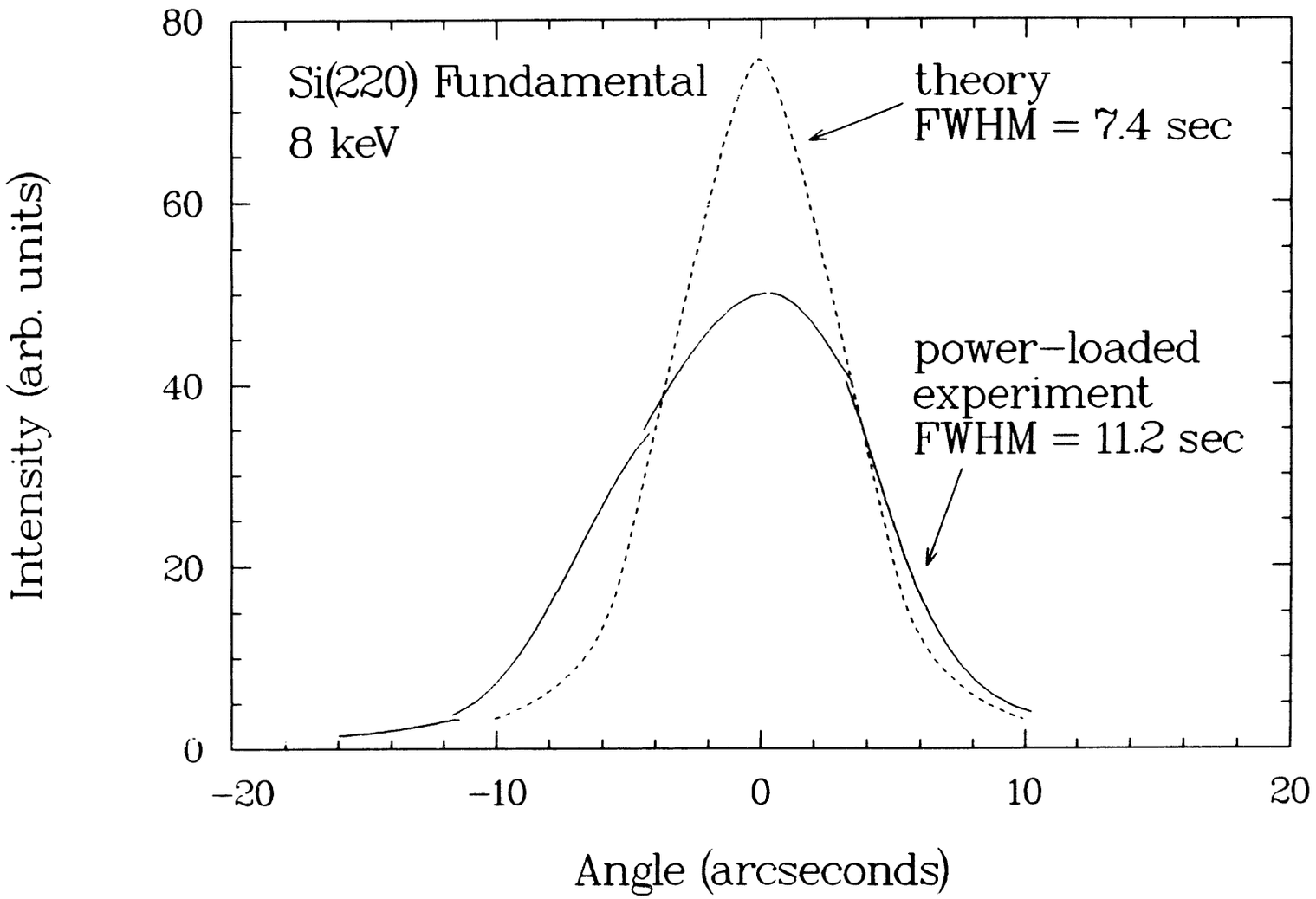

Berman et al., SRI-91 contribution S11, Figure 3 upper panel

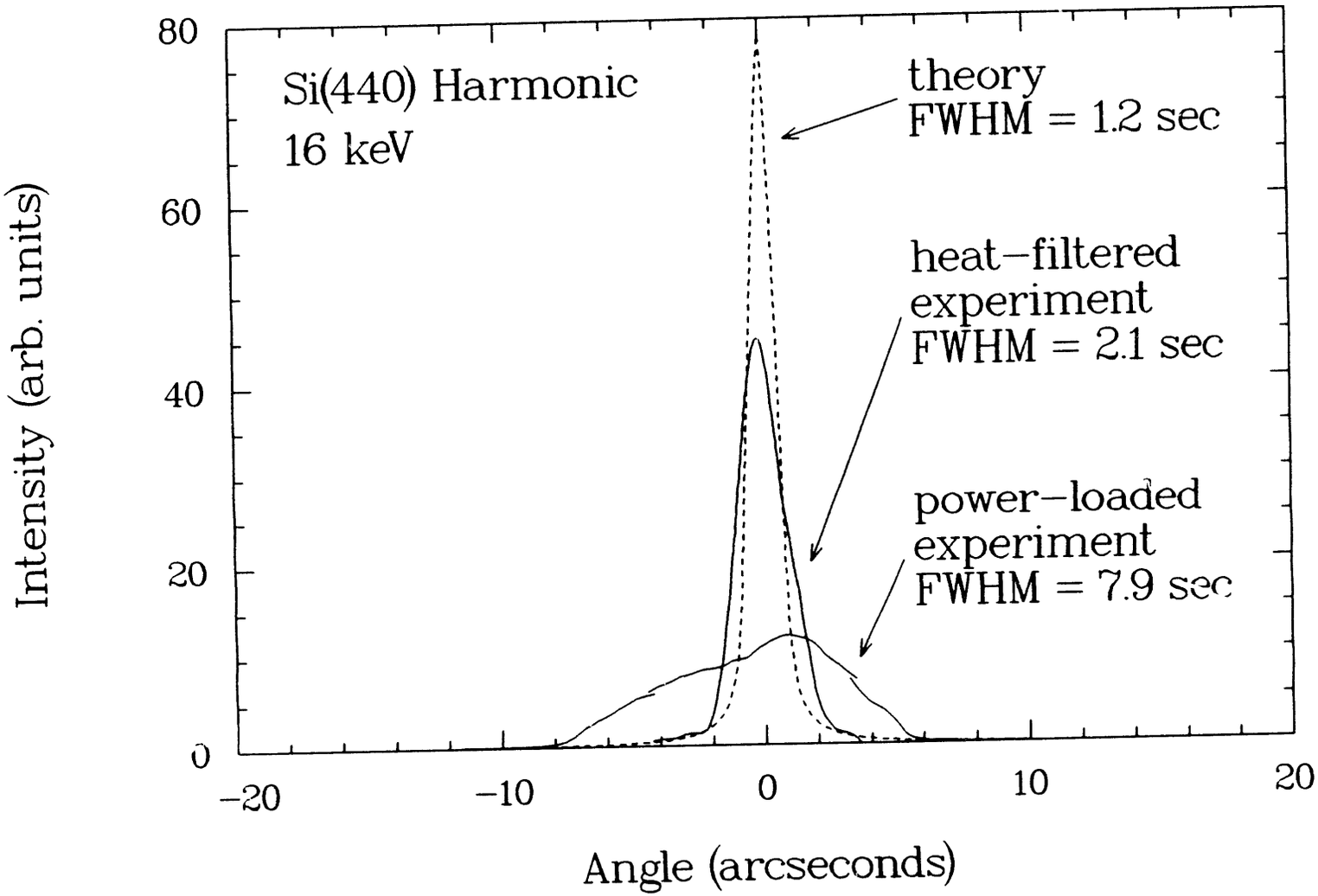

Berman et al., SRI-91 contribution S11, Figure 3 lower panel

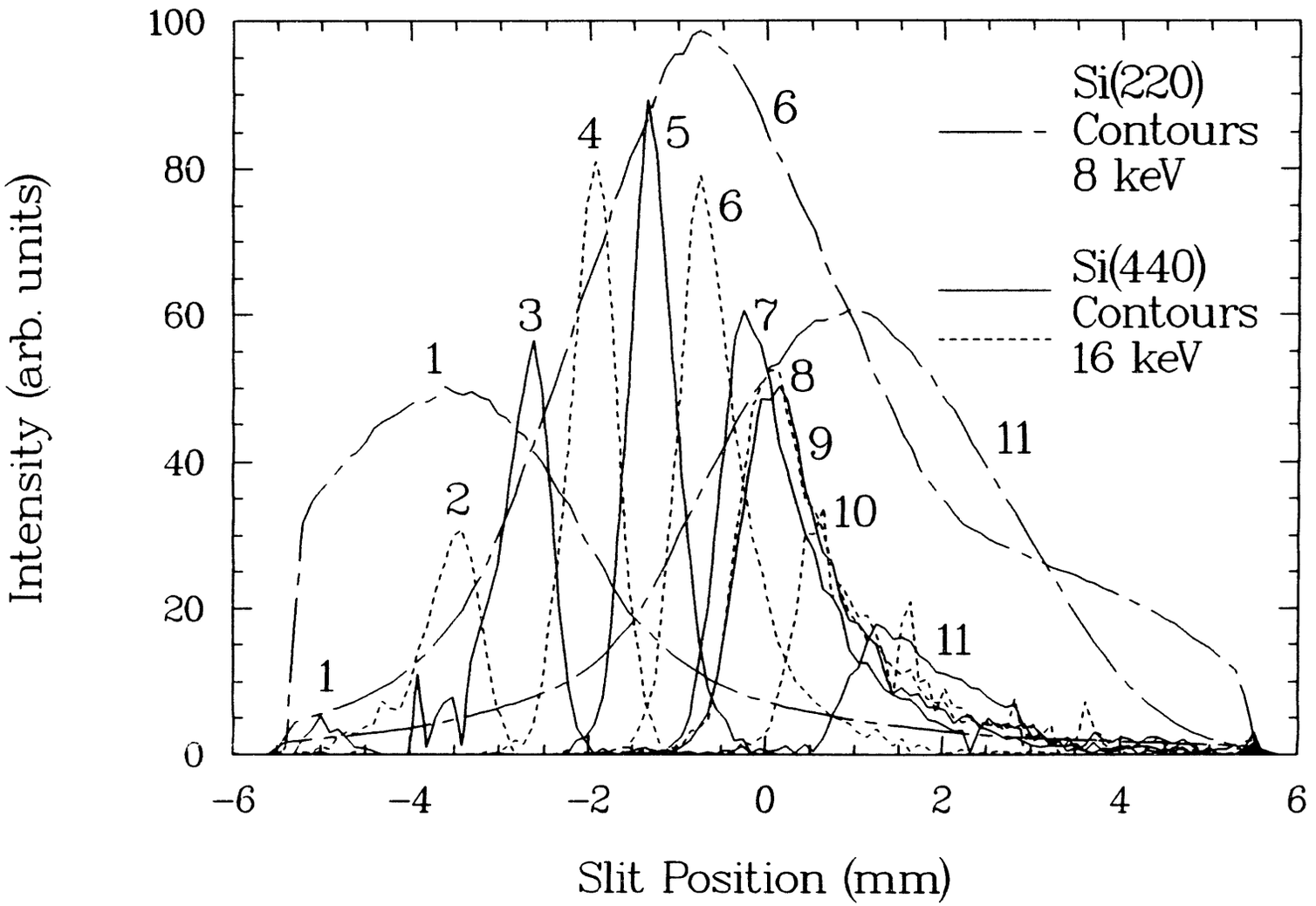

Berman et al., SRI-91 contribution S11, Figure 4

END

DATE FILMED

11/27/91